Journal of Cellular Biochemistry 102:64–74 (2007)

Intracoronary Delivery of Autologous Bone Marrow Mononuclear Cells Radiolabeled by 18F-Fluoro-Deoxy-Glucose: Tissue Distribution and Impact on Post-Infarct Swine Hearts

Haiyan Qian,[1] Yuejin Yang,[1]* Ji Huang,[2] Runlin Gao,[1] Kefei Dou,[1] Guosheng Yang,[1] Jianjun Li,[1] Rui Shen,[3] Zuoxiang He,[3] Minjie Lu,[4] and Shihua Zhao[4]

[1]Department of Cardiology, Fuwai Hospital and Cardiovascular Institute, Peking Union Medical College and Chinese Academy of Medical Sciences, Beijing, P.R. China
[2]Department of Cardiology, Renmin Hospital of Wuhan University, Wuhan, P.R. China
[3]Department of Nuclear Medicine, Fuwai Hospital and Cardiovascular Institute, Peking Union Medical College and Chinese Academy of Medical Sciences, Beijing, P.R. China
[4]Department of Radiology, Fuwai Hospital and Cardiovascular Institute, Peking Union Medical College and Chinese Academy of Medical Sciences, Beijing, P.R. China

Abstract Intracoronary injection of the bone marrow-derived mononuclear cells (MNCs) is emerging as a potentially novel therapy for ischemic heart failure. This study was aimed at assessing the efficacy of intracoronary MNC delivery in the myocardium. The in vivo distribution and myocardial homing of intracoronarily delivered MNCs in experimental Chinese swine with acute myocardial infarction (AMI) created by occlusion of left anterior descending (LAD) coronary artery for 90 min. MNCs radiolabeled with 18F-fluoro-deoxy-glucose (18F-FDG) were delivered using a coronary catheter into the infarct-related coronary artery 1 week after AMI. Dual-nuclide single photon emission computed tomography (SPECT) revealed that 1 h after cell infusion, $6.8 \pm 1.8\%$ of 18F-FDG-labeled MNCs occurred in the infarcted myocardium with the remaining activity found primarily in the liver and spleen. In the heart, MNCs were detected predominantly in the under-perfused myocardium. The infused cells retained in the hearts at a rate highly correlated with the under-perfused lesional sizes. Pathological examination further demonstrated that 6 weeks after infusion, compared to controls, the hearts receiving MNCs exhibited less fibrosis and inflammatory infiltrate, more viable tissue, and higher vascular density. Cardiac function was significantly improved in the MNC-infused hearts. Thus, 18F-FDG labeling and dual-nuclide SPECT imaging is capable of monitoring in vivo distribution and homing of MNCs after intracoronary infusion. MNC coronary delivery may improve cardiac function and positive ventricular remodeling in the heart with AMI. J. Cell. Biochem. 102: 64–74, 2007.

Key words: mononuclear cells; transplantation; acute myocardial infarction; distribution; single photon emission computed tomography; 18F-fluoro-deoxy-glucose

Recently, experimental studies and clinical trials have indicated that cellular cardiomyoplasty with stem cells may have benefits on tissue perfusion and contractile performance of the injured heart [Fernandez-Aviles et al., 2004; Schuster et al., 2004]. With respect to the donor cells, investigators have practically chosen bone marrow-derived mononuclear cells (MNCs) [Kocher et al., 2001; Tse et al., 2003; Perin et al., 2004], which contain different types of stem cells, including hematopoietic stem cells, endothelial progenitor cells, and mesenchymal

Grant sponsor: Ministry of Science and Technology of China; Grant number: 2005CB523303.

*Correspondence to: Yuejin Yang, MD, PhD, Department of Cardiology, Fuwai Hospital, Peking Union Medical College and Chinese Academy of Medical Sciences, 167 BeiLiShi Rd., Beijing 100037, P.R. China.
E-mail: Dr_yuejinyang@yahoo.com.cn

Received 17 October 2006; Accepted 29 December 2006
DOI 10.1002/jcb.21277

stem cells. Relatively higher availability and no need for in vitro expansion are additional advantages of using MNCs.

Among several delivery routes of donor cells into the targeted area, intracoronary infusion is especially suitable to clinical settings. In this procedure, cells were delivered through the over-the-wire balloon catheter during transient balloon inflations to maximize the contact time of stem cells with the vascular walls of the infarct-related area. Infusion in the infarct-related artery allows the stem cells to transmigrate the vascular walls into the peri-infarct region, which differs from intramyocardial injection that may lead to disperse islands of cells in the infarct-related region, which may serve as a potential source for arrhythmias [Strauer et al., 2002; Britten et al., 2003; Wollert et al., 2004].

Some of the infused cells will be flushed away from the coronary circulation by blood flow. Therefore, only a portion of the infused cells are entrapped in the heart. It is not clear how many of the stem cells intracoronarily delivered will migrate or home into the targeted region. Hofmann et al. [2005] for the first time clinically monitored the distribution of bone marrow cells (BMCs) radiolabel by 18F-fluoro-deoxy-glucose (18F-FDG) under positron emission tomography imaging (PET). Then several studies suggested that radioactive isotopes such as ^{99m}Tc-HMPAO and ^{111}In-oxine can be used to label donor cells, thus systematic biodistribution of donor cells can be detected in vivo in animal models and patients with MI [Hou et al., 2005; Kang et al., 2006]. Because of the difference in the labeling methods and in the types of donor cells used in the studies, the results from previous studies appear very discrepant. Since current clinical studies have shown that bone marrow-derived MNCs are beneficial to the infarcted hearts, the bone marrow-derived MNCs delivered to the heart by intracoronary infusion are likely to exist in the heart, and exert their tissue-repair or regenerative function. In addition, it is very important not only to determine the tissue distribution of implanted stem cells in vivo, but also disclose the impacts of infused cells on cardiac function in the hearts with AMI.

The current study was designed to determine: (1) the systematic distribution and myocardial localization of intracoronarily delivered bone marrow-derived MNCs by dual-nuclide single photon emission computed tomography (SPECT) scanning in vivo; (2) the effects of intracoronary infusion of autologous bone marrow-derived MNCs on post-infarction swine hearts.

MATERIALS AND METHODS

Animals

Fourteen Chinese mini-pigs (30 ± 5 kg) with the age of 10 months old were obtained from laboratorial animal center of Chinese University of Agriculture. All animals received human care in compliance with the Guide for the Care and Use of Laboratory Animals published by US National Institute of Health. Also, all experimental procedures have been approved by the Care of Experimental Animals Committee of Chinese Academy of Medical Sciences and Peking Union Medical College, China.

Isolation of Porcine Bone Marrow-Derived Mononuclear Cells (MNCs)

Swine were sedated with ketamine (25 mg/kg intramuscular) and valium (1 mg/kg). About 50 ml of bone marrow was aspirated from left iliac crest into a syringe containing 12,500 units of heparin. All animals received buprenorphine (0.3 mg intramuscular) as an analgesic before returning to the animal facility.

The marrow aspirates were then prepared for MNC isolation as previously described with some modifications. Briefly, the bone marrow aspirates were doubly diluted with phosphate buffer saline (PBS), and then centrifuged through density gradient centrifugation with 1.077g/ml Percoll (Sigma). The cellular pellets were then rinsed twice with low-glucose DMEM (Gibco).

Myocardial Infarction and Transplantation of MNCs

Swine were sedated with ketamine (25 mg/kg intramuscular), induced with valium (1 mg/kg), endotracheally intubated and mechanically ventilated with a Narkomed ventilator, and maintained anesthesia through intravascular injection of ketamine and valium. A midline sternotomy was performed and the heart suspended in a pericardial cradle. The left anterior descending (LAD) coronary artery was dissected free just distal to the first diagonal branch and isolated with a vessel loop. An occlusion of the coronary artery was performed to identify the region to be rendered ischemic. A 90-min occlusion of the LAD was used to produce myocardial infarction. Following the

baseline recording and in the end of occlusion, the snare was released and reperfusion was visually confirmed. The anesthetic was then stopped, the animal extubated when appropriate, and allowed to recover. Animals received postoperative antimicrobial therapy (cephazoline 1.0 intramuscular twice daily for 3 days) and buprenorphine (0.3 mg IM twice daily for 3 days) for postoperative pain.

The cells were labeled with 4′,6-diamidino-2-phenylindole (DAPI; Sigma) for 30 min at 37°C. The cells were rinsed six times in DMEM to remove unbound DAPI (1.0×10^9 cells for every animal). This labeling procedure was very efficient, ensuring almost 100% labeling of cell nuclei. For radiolabeling of MNCs with 18F-FDG, MNCs were incubated under sterile conditions in a 10-ml test tube with 185 MBq 18F-FDG (5 mCi) for 30 min at 28°C under gentle rolling in serum-free PBS (pH 7.2) containing 10 U/ml heparin (Roche) and 0.1 U/ml recombinant human insulin (Novo Nordisk). To remove excess unbound 18F-FDG, cells were subjected to a centrifugation and washing process in heparinized PBS (60g; 120 s). Radioactivity in the supernatant and cell pellet was measured with a dose calibrator (Capintec). 18F-FDG-labeled cells were resuspended in 10 ml heparinized (10 U/ml) saline before application. Cell viability was assessed by trypan blue dye exclusion assay right before infusion.

Fourteen pigs were divided into two groups, including group 1 = control (n = 7), group 2 = transplantation of MNCs (n = 7). Just after 1 week after AMI, the transplantation was conducted. Autologous MNCs (1.0×10^9 cells/10 ml) were infused into the LAD artery using an over-the-wire balloon catheter placed within the LAD just distal to the 1st diagonal branch in group 2. With 4 to 6 atm pressure inflation in the balloon catheter, 10 ml of cell suspension (1×10^9 cells) was infused over 5 min. Ballooning prevented cell backflow and at the same time produced a stop-flow beyond the site of the balloon inflation to facilitate high-pressure infusion of cells into the infarcted zone. In group control, the same volume of PBS was intracoronarily delivered similar to above procedures.

Tissue Distribution of Infused MNCs by Dual-Nuclide SPECT Imaging

^{18}F-FDG-labeled MNCs were administered by over-the-wire angioplasty balloon catheter through coronary catheterization performed 1 week after infarction. A dose of 296MBq (8mCi) ^{99m}Tc-sestamibi was injected intravenously sequentially.

After 1 h of stem cell infusion, whole-body planar images were acquired with the dual-head gamma camera (Millennium^{TM} VG, GE). SPECT was performed using ultra-high energy collimators (VP94, GE). Energy discrimination was provided by 20% windows centered on 140 keV for ^{99m}Tc and 511 keV for ^{18}F, respectively, with a matrix of 128×128.

Dual-isotope myocardial SPECT were performed close behind whole-body planar images. Thirty projections over 180° arcs were acquired with 40 s per projection. A zoom factor of 1.25 and a matrix of 64×64 were used. Imaging data were reconstructed with filtered back-projection algorithm. Butterworth filter with an order 5 and cutoff frequency 0.50 were using for imaging interpretation.

Whole-body images were analyzed by region of interest (ROI) technique. ROI was drawn manually on lung, heart, liver, spleen, kidney and peripheral circulation on ^{18}F-FDG-labeled MNCs imaging, which was in accordance with ^{99m}Tc-sestamibi imaging for anatomic localization. Total and mean radioactivity of each organ was calculated from anterior imaging. Myocardial SPECT images were interpreted by two nuclear cardiologists, for determination of location of myocardial infarction and aggregation of ^{18}F-FDG-labeled MNCs in myocardium.

Assessment of Cardiac Function by Magnetic Resonance Imaging (MRI) and SPECT

Animals were studied 1 week after infarction (baseline) and 6 weeks after cell transplantation (endpoint) by cine MRI and contrast enhancement MRI (CE MRI). MRI was performed using a 1.5 T clinical MRI scanner (Siemens Avanto) with a phase array radiofrequency receiver coil. Animals were sedated with ketamine (25 mg/kg i.m.) and valium (1 mg/kg i.m.). MRIs were wireless vector ECG gated. Both cine and corresponding CE MRI were prescribed every 4 mm from base to apex, starting at the level of the mitral valve, which resulted in 6–8 short axis slices. Scout transversal and sagittal views ensured correct determination of the short-axis planes. Several long axis cine about every 60 was also prescribed. Cine MRI images were acquired using a TrueFisp sequence with time-adaptive sensitivity encoding (TSENSE)

technique. Typical imaging parameters were the following: repetition time, 35 ms; echo time, 4.8 ms; bandwidth, 195 kHz; flip angle, 30j; in plane resolution, 0.3 mm × 0.3 mm and slice thickness, 2 mm. CE MRI was performed directly after administration of 0.2 mmol/kg Gd-DTPA (Magnevist®, Schering®). T1-weighting was achieved using a phase sensitivity inversion recovery (PSIR) FLASH sequence. Inversion time (TI) was auto-adjusted by PSIR technique. Typical image parameters were: repetition time, 1,350 ms; echo time, 4.8 ms; bandwidth, 130 kHz; in plane resolution, 0.3 mm × 0.3 mm and slice thickness, 2 mm. Six weeks after injection all cine and CE MRI images were repeated (endpoint). Those short axis slices were imaged in corresponding to the slices at baseline based upon anatomical landmarks. Additionally, to provide healthy controls, five sham animals were studied by cine MRI following the same MRI protocol.

To determine myocardial perfusion, myocardial SPECT were performed at both 1 week after myocardial infarction induction (baseline) and 6 weeks after delivery of MNCs (endpoint). For SPECT 99mTc-sestamibi, about 296 MBq (8 mCi) was administered to the pigs and the hearts were imaged 45–60 min later with a gamma camera. The dual head gamma camera (Varicum, GE) with a low energy, a high resolution collimator with a 20% energy window was set to 140 keV gamma peak. Thirty-two projection images per 40 s in a 64 × 64 matrix were achieved by using a 180-rotation arc from the 45-right and anterior sector to the 45-left and anterior sector. SPECT was reconstructed with Butterworth cut-off frequency of 0.45, with an order of 5 and the reconstructed data were created along three oblique axis (short axis, vertical long axis, and horizontal long axis) planes by setting the axes of the heart. Quantitative analysis was performed using Cedars quantitative perfusion SPECT (QPS). Perfusion defects were calculated using a scintigraphic bull's eye technique.

Immunohistochemistry Analysis

To determine in vivo cardiomyogenic differentiation and angiogenesis in the hearts with implanted MNCs, the heart tissue was cryosectioned at 5 μm and stained with antibodies for the endothelial cell marker Von Willebrand factor (VWF, 1:50, DAKO), vascular smooth muscle-specific α-actin (SM-actin, 1:50, DAKO), and the cardiac markers, for example, α-sarcomeric actin (1:50, DAKO), cardiac troponin T (1:50, Sigma), connexin 43 (1:50, Sigma). After washing with PBS, sections were incubated with a goat anti-mouse conjugated rhodamine IgG or a goat anti-rabbit conjugated FITC IgG. Finally, fluorescent staining were detected and photographed under laser scanning confocal microscope.

To determine the vascular density in infarcted myocardium and in peri-infarct zone, tissue was prepared as described previously [Weidner et al., 1991]. Sections were stained using polyclonal VWF antibody (1:200, DAKO). For quantification of positively stained vessels, five sections from within the infarct zone and eight from within the peri-infarction zone of each animal were analysed by independent investigators who were blinded with respect to the treatment. Microvessles were counted in five randomly chosen high-power fields (HPFs) in every chosen section. The results were expressed as microvessels per high power field.

Statistics

Continuous variables are presented as means ± standard deviation. After having evaluated the homogeneity of variance and normal distribution of data, analysis of variance was performed to determine differences among groups in each stage of analysis (baseline and endpoint), and adjusted to baseline results for a endpoint analysis. Comparison of MRI and M-SPECT parameters between baseline and endpoint and between groups were evaluated by paired and unpaired Student's *t*-test, respectively. Values were considered significantly different when $P < 0.05$ after Bonferroni's correction. When frequency data were compared, the nonparametric Fisher's exact test with the 0.05 level of probability was used. All statistical analyses were conducted with SPSS 13.0.

RESULTS

MNCs Labeling With 18F-FDG and Distribution of Infused Cells

Immediately after radiolabeling, MNC viability was examined, which showed more than 97% viable cells, similar to those found in the cells unlabeled with 18F-FDG. Under the condition of radiolabeling, the labeled MNCs had the viability at more than 93% viability, indicating that radiolabeling is a mild process doing

little harm to the BMCs. In all the applications, the radioactivity in the MNCs after incubation with ^{18}F-FDG was $90.8 \pm 1.9\%$ of the total radioactivity.

One hour after cell infusion, $6.8 \pm 1.8\%$ of 18F-FDG-labeled MNCs appeared in the infarcted myocardium. More than 90% of the radioactivity accumulated in the liver and spleen (Fig. 1A). There was no significant retention of radiolabeled MNCs in the lungs. Radioactivity retention in the myocardium after intracoronary infusion of ^{18}F-FDG-labeled MNCs was $6.8 \pm 1.8\%$ in all animals with MI. In all six animals, radioactivity in the heart was localized in only the zone of perfusion defect; no significant activity was detected in other regions of the myocardium (Fig. 1B). It is interesting that the retention rate of MNCs in heart was positively correlated with the area of perfusion defect ($P = 0.001$, Pearson correlation = 0.973, Fig. 1C). Labeling details and distribution data are presented in Table I.

Cardiac Function Assessment by MRI and SPECT

Changes in LV function and geometry in the transplantation and control group are shown (Table II). Cardiac function parameters at baseline, including left ventricular ejection fraction (LVEF), end-diastolic volume (EDV), end-systolic volume (ESV) infarction size, dyskinetic segments, wall thickening, and left ventricular mass index (LV mass index) were not significantly different between the control and stem cell groups.

In the endpoint, LVEF changed by 0.7 and 7.3% in group control and group 2, respectively, there is a significant difference ($P = 0.011$). A total of 36 segments were analyzed in the control and cell-implanted groups, respectively, and those dyskinetic segments were used for analysis of wall thickening. All segments with dyskinesia were used for calculation of regional wall thickening. The regional wall thickening was further decreased in the control group to $-22.3 \pm 5.7\%$, whereas in the group 2 were significantly increased to $45.7 \pm 11.1\%$ ($P < 0.0001$), indicating that a severe impairment in wall thickening is visible in the control animals at the site of the infarct, whereas in the MNCs-treated animals, regional wall thickening at the infarct level is significantly improved. Although EDV had not significant decrease in group 2 compared with that in group control at endpoint ($P = 0.196$), ESV decreased

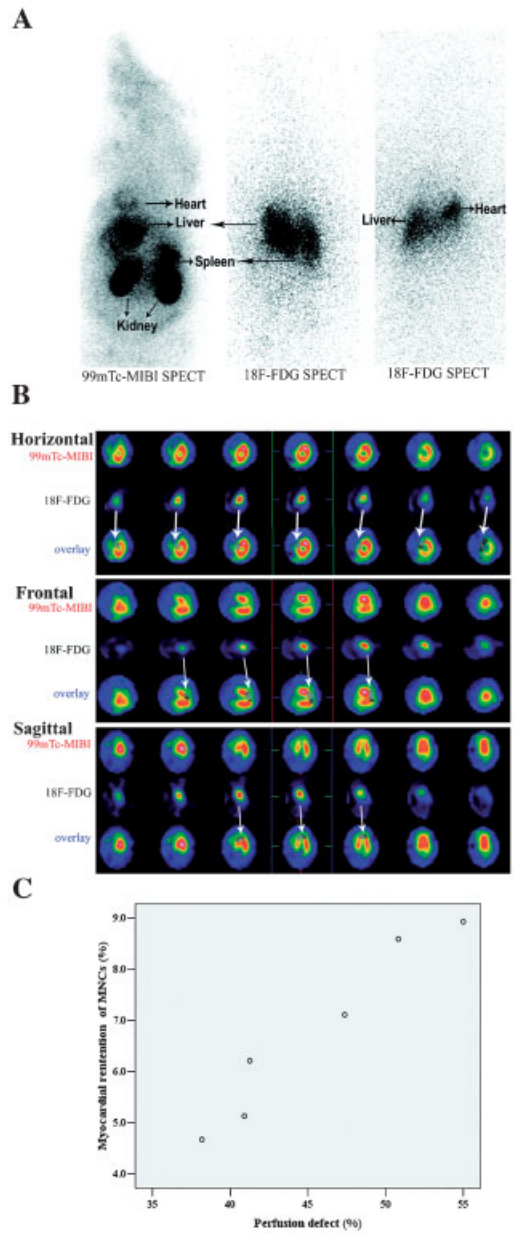

Fig. 1. Early distribution of 18F-FDG-labeled MNCs after intracoronary delivery by dual-nuclide SPECT scanning in vivo. **A**: Systematic dual-nuclide SPECT image showed the distribution of MNCs in the organs. 18F-FDG SPECT scannings in vivo that showed organ retention of radiolabeled MNCs at the similar body position to 99mTc MIBI-SPECT imaging. Images showed that 18F-FDG-labeled MNCs predominantly accumulated in the liver, then in the spleen and the heart. **B**: Intramyocardial localization of 18F-FDG-labeled MNCs. Cardiac tomoscan with 99mTc-MIBI SPECT (the first, fourth, and seventh row) showed the localization of perfusion defect, and at the similar cardiac slices, overlaying pictures (the third, sixth, and ninth row) showed that 18F-FDG-labeled MNCs most deposited in infarct center and peri-infarct zone, rather than in normal myocardium. **C**: The retention rate of MNCs homing in myocardium was positively correlated with the size of perfusion defect ($P = 0.001$, Pearson correlation = 0.973).

TABLE I. Radiolabeling Efficiency and Distribution of MNCs In Vivo

Animal number	1	2	3	4	5	6	Mean ± SD
Number of MNCs ($\times 10^9$)	1.0	1.0	1.0	1.0	1.0	1.0	
Supernatant radioactivity (mCi)	0.22	0.17	0.26	0.18	0.21	0.29	0.22 ± 0.05
MNC-abound radioactivity (mCi)	2.19	2.13	2.09	2.23	2.24	2.13	2.17 ± 0.06
Radiolabeling efficiency (%)	90.87	92.61	88.94	92.53	91.43	88.17	90.76 ± 1.85
Percentage of systematic retention							
Heart (%)	6.2	8.6	8.9	5.1	7.1	4.7	6.8 ± 1.8
Liver (%)	72.1	66.2	63.7	65.6	68.4	70.2	67.7 ± 3.1
Spleen (%)	15.8	16.5	17.9	18.4	16.9	18.6	17.3 ± 1.1
Peripheral circulation (%)	5.9	8.7	9.5	10.9	7.7	6.5	8.2 ± 1.9

significantly in group 2 compared with control ($P = 0.039$), indicating that cell therapy improved left ventricular systolic function. The functional improvement in the MNCs group was further accompanied by prevention of LV remodeling as indicated by smaller LV mass index compared with group control at endpoint ($P = 0.012$), as so less infracted size ($P < 0.0001$) (Fig. 2).

Figure 3 displays representative SPECT images taken from the area with the perfusion defect before and after MNC delivery. Initial baseline SPECT findings demonstrate no significant differences between 2 groups (47.1 ± 7.5% vs. 45.6 ± 6.6%, $P = 0.713$). However, 6 weeks after MNCs implantation, follow-up SPECT showed the mean area of perfusion defect changed to 44.8 ± 6.7%, 23.9 ± 5.1% in groups control and group 2, respectively (each n = 6, $P < 0.0001$).

Histological Findings

H&E staining showed that severe fibrosis and scarce surviving myocardium could be observed in infarcted zone in group control. In contrast, the extent of fibrosis in group 2 was significant less than that in group control (Fig. 4A).

Six weeks after transplantation of MNCs, immunofluorescent analysis in frozen sections indicated that DAPI positive cells expressed cardiac- and microvessel-specific proteins, including α-sarcomeric actin, cardiac troponin T, connexin 43, Von Willebrand factor, and vascular smooth muscle actin, in group 2, which demonstrated that implanted MNCs had already differentiated to cardiomyocytes and microvessels (Fig. 4B,C).

Vascular Density

Vascular density in the infarcted zone as well as in peri-infarct zone was determined following immunostaining with VWF antibody. There were a significant difference in vascular densities in infarcted zone between group control and group 2 (1.8 ± 0.5/HPF vs. 3.7 ± 1.1, $P < 0.003$). In peri-infarct area, vascular density was 8.7 ± 2.0/HPF in group 2, which was again significantly more than that in group control (4.9 ± 1.3/HPF, $P < 0.003$) (Fig. 5).

DISCUSSION

Recent studies have shown that intracoronary delivery of autologous bone marrow-derived MNCs can beneficially affect the ventricular

TABLE II. Assessment of Left Ventricle Function by MRI

	Control (n = 6)		Group 2 (n = 6)	
Group	Baseline	Endpoint	Baseline	Endpoint
Global LVEF (%)	43.5 ± 7.3	44.2 ± 8.2	43.9 ± 8.5	51.2 ± 10.4*
EDV (ml)	58.8 ± 6.6	68.7 ± 5.3	56.2 ± 8.4	63.3 ± 7.8#
ESV (ml)	34.7 ± 6.4	38.5 ± 7.3	32.0 ± 10.1	31.5 ± 10.3*
Dyskinesia segments	7.8 ± 1.0	7.2 ± 0.8	8.2 ± 1.2	4.8 ± 0.8*
Wall thickening in dyskinetic segments (%)	−17.5 ± 6.3	−22.3 ± 5.7	−18.2 ± 7.3	45.7 ± 11.1*
Infarct size (cm^2)	6.6 ± 0.8	6.9 ± 0.4	6.9 ± 1.1	3.7 ± 0.7*
LVmass (g/m^2)	61.7 ± 7.2	72.7 ± 4.6	59.8 ± 8.9	64.2 ± 7.9*

LVEF, left ventricular ejection fraction; EDV, end-diastolic volume; ESV, end-systolic volume.
*$P < 0.05$ (comparison of values at endpoint, group control vs. group 2).
#$P = 0.196$ (comparison of EDV at endpoint, group control vs. group 2).

remodeling process and improve cardiac function after MI [Kamihata et al., 2001; Tse et al., 2003; Perin et al., 2004]. Intracoronary cell infusion is a popular approach, because of the familiarity of most cardiologists with this well-established procedure, however, the precise quantification of infused cells in targeted area of myocardium in vivo is not clear. Several studies investigate the distribution of implanted cells transfected with reporter genes based on the histological level, however, which is not precise and unsuitable for clinical situation [Allers et al., 2004; Suzuki et al., 2004]. Therefore, it is very important to detect distribution of implanted cells in living body in vivo. The rapid development of nuclear medicine paves a way for the study of distribution of implanted cells in vivo.

Radiolabeling of leukocytes is an established method to localize areas of infection and inflammation in vivo. Of the different labeling nuclides, ^{18}F-FDG provides superior image quality [Becker and Meller, 2001]. As shown in the study by Hofmann et al. [2005], they determined that after intracoronary delivery, 1.3–2.6% of 18F-FDG-labeled unselected BMCs were detected in the infarcted myocardium; the remaining activity was found primarily in liver and spleen. Penicka et al. [2005] indicated that the radioactivity uptaked by the heart was 5% of the ^{99m}Tc-HMPAO-labeled BMCs at 1 h after intracoronary transplantation in one patient with AMI, and the majority of transplanted BMCs were accumulated in spleen. Kang et al. [2006] injected 18F-FDG-labeled stem cells via an intracoronary catheter, and PET/CT images showed 1.5% (range, 0.2–3.3%) of injected stem cells accumulated at the infarcted myocardium 2 h after intracoronary infusion. Outside of the myocardium, spleen, liver, bladder, and bone marrow showed a high stem cell accumulation. The delayed image of a patient up to 20 h showed a prolonged residence of stem cells at the myocardium. Hou et al. [2005] found the remarkable feature of intracoronary delivery

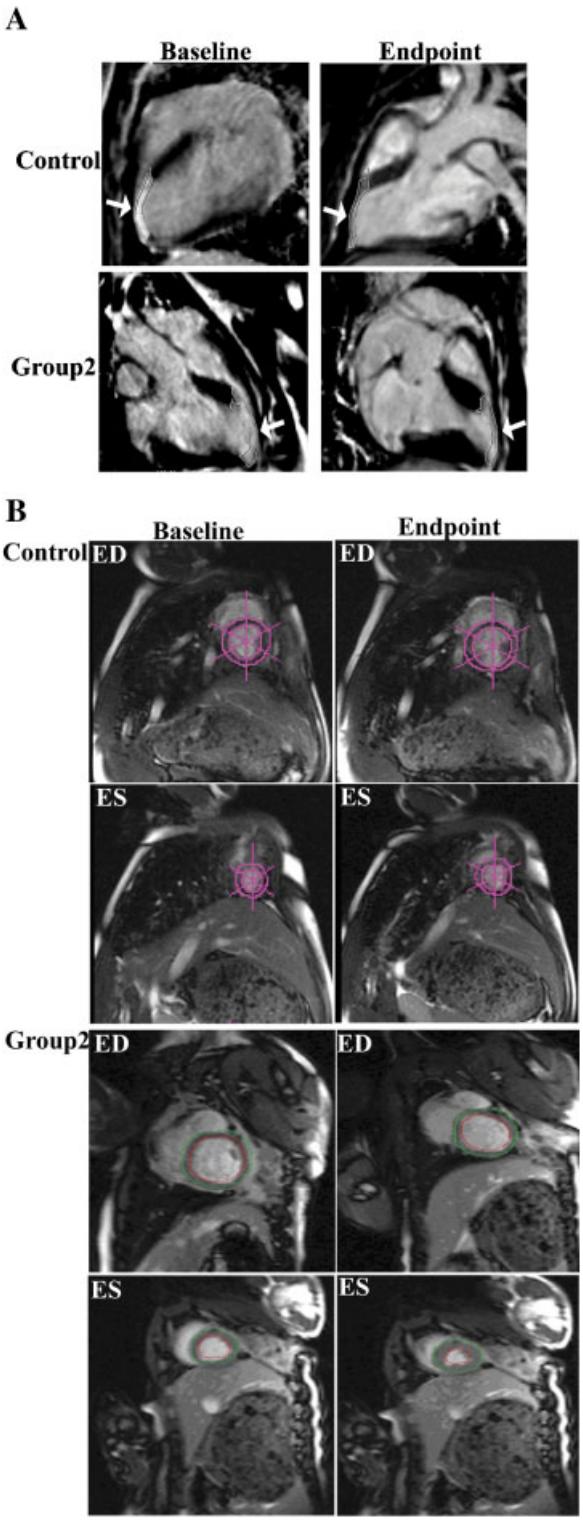

Fig. 2. Representative pictures of MRI imaging. **A**: showed that infarcted size (arrow) by late enhancement imaging, and there was not significant difference in between the baseline and the endpoint in group control (6.6 ± 0.8 cm^2 vs. 6.9 ± 0.4 cm^2, $P = 0.604$), however, the infarcted size remarkably decreased in the endpoint in group 2 (6.9 ± 1.1 cm^2 vs. 3.7 ± 0.7 cm^2, $P < 0.0001$). **B**: showed that the wall thickening of infarction-related regions in the baseline and endpoint. There were not significant changes from baseline to endpoint in group control ($-17.5 \pm 6.3\%$ vs. $-22.3 \pm 5.7\%$, $P = 0.869$), however, the wall thickening of infarction-related regions in group 2 increased significantly ($-18.2 \pm 7.3\%$ vs. $45.7 \pm 11.1\%$, $P < 0.0001$). ED, end-diastolic phase; ES, end-systolic phase. [Color figure can be viewed in the online issue, which is available at www.interscience.wiley.com.]

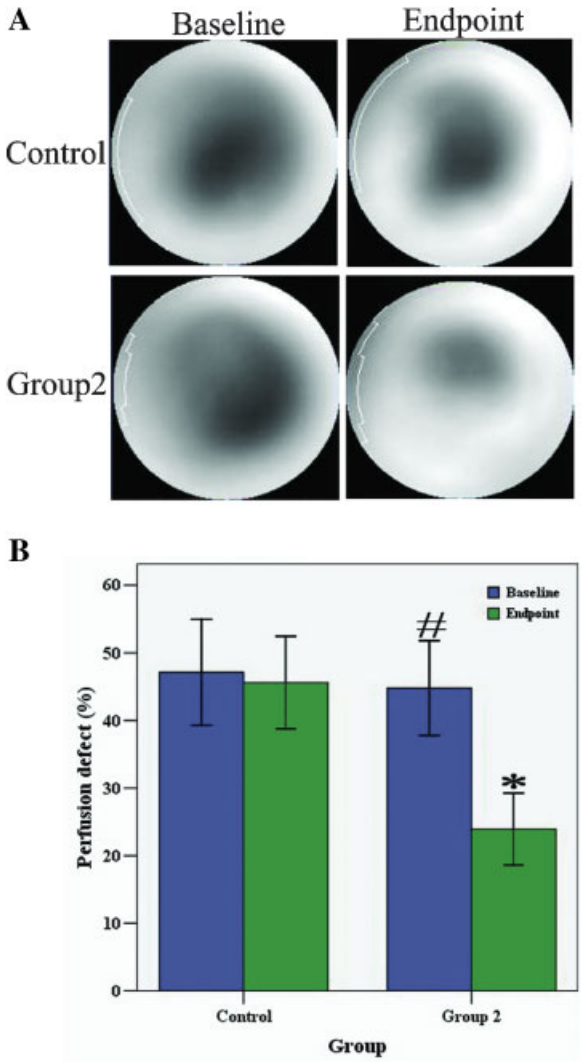

Fig. 3. Assessment of perfusion defect of left ventricles by ^{99m}Tc-MIBI SPECT in the baseline and endpoint. **A**: Representative figures about perfusion defect in group control and group 2 in the baseline and endpoint. **B**: Statistics figure of perfusion defect in group control and group 2 in the baseline and endpoint. Comparison of values in the baseline with that in the endpoint, $^{\#}P = 0.713$ (comparison of values in the baseline, group control vs. group 2); $^{*}P < 0.0001$, (comparison of values in the endpoint, group 2 vs. group control). [Color figure can be viewed in the online issue, which is available at www.interscience.wiley.com.]

was the largely right-sided distribution of cells, marked by pulmonary cell trapping far in excess of that by filter organs (e.g., liver and spleen) on the systemic/left-sided circulation.

However, these studies did not investigate the effects of implanted cells labeled by radioactive isotopes on cardiac function of AMI. In addition, the studies by Penicka et al. [2005] and Kang et al. [2006] showed that the significant accumulation of radioactivity in the bladder, which indicate that some fraction of nuclides are not uptaked by stem cells, thus resulting in the un-precise calculation of distribution in vivo.

In the present study, dual-nuclide SPECT was used in the swine infarction model to assess the early retention of 18F-FDG-labelled MNCs, after these cells had been intracoronarily injected. Moreover, the retention localization could be assessed, because of the additional recording of sestamibi SPECT at the same time of cell transplantation. In previous studies, although injected cells were found to accumulate in the damaged heart, it was not known whether they were truly present in the targeted MI area. Our results demonstrate that homing MNCs in myocardium mainly localize the region of perfusion defect, which is consistent with the report by Hofmann et al. [2005], indicating the functional benefits resulting from cell therapy occur in the infarcted and peri-infarcted region. In addition, the most interesting finding of our study is that the retention rate of infused cells in myocardium has a significantly positive correlation with the size of perfusion defect at SPECT. The result maybe indicate that signals in the local microenvironments of infarcted myocardium are more powerful in those animals with larger size of MI than that in animals with less MI, and it is the signals that attract infused cells homing into the targeted area. In addition, we did not find the retention of infused cells in the lungs, which is not consistent with previous studies. It is not clear what causes this difference.

In this study, we detected a relatively higher retention rate of infused MNCs in the myocardium with infarction. According to the finding that the retention rate is positively correlated with under-perfusion area, the size of under-perfusion in our study is about $45.6 \pm 6.6\%$ at SPECT, which is significant more than that in other research results.

Compared with other radioactive tracers, 18F-FDG has remarkable advantages, including availability and ease of use, very low concentrations needed for imaging, and long positron range of the emitted β-particle (≈ 0.5 mm). Moreover, the slight toxicity to cells is the additional advantage. Because of the physical half-life (110 min) of 18F, we could not assess distribution and myocardial localization of MNCs days later. Although indium oxine imaging has the advantage of delayed imaging

because of its longer half-life, poor resolution and higher radiation exposure might limit human application. Now, the size of stem cells, acquisition time after injection, and method of injection may affect the results, and further comparison studies are needed to determine which cell types are homing better at the target tissue.

Bone marrow-derived MNCs represent a mixed population of various stem cells, stromal cells, and hematopoietic cells at various maturation stages. It is not yet clear which cell population(s) promote functional recovery in patients after intracoronary infusion. In experimental models of AMI, functional improvements have been reported after transplantation of unselected or highly selected BMC populations, including endothelial progenitor cells, hematopoietic stem cells, and mesenchymal stem cells [Kamihata et al., 2001].

Our results demonstrate that the intracoronary transplantation of autologous bone marrow MNCs may reduce infarct size and improve LV function. Although EDV in group 2 did not significantly decrease compared with group control at endpoint, the decrease of infarct size, number of dyskinetic segments, ESV and left ventricular mass index, and the increase of LVEF and wall thickening in dyekinetic area in all animals of group 2 are significant compared with that in control group. The effects of stem cell transplantation are demonstrated by significant improvement of these parameters in the therapy group (before and after stem cell therapy) as well as in the comparison between the stem cell therapy group and the control group, thus giving evidence for a beneficial therapeutic effect of stem cell therapy on cardiac performance in AMI.

The regenerative potential of bone marrow-derived stem cells may be interpreted by the following mechanisms: (1) transdifferentiation from mononuclear cells into cardiomyocytes [Beltrami et al., 2003], (2) angiogenesis [Tang et al., 2004], (3) paracrine-induced increase of residual viable myocytes [Orlic et al., 2001], (4) stimulation of intrinsic myocardial stem cells

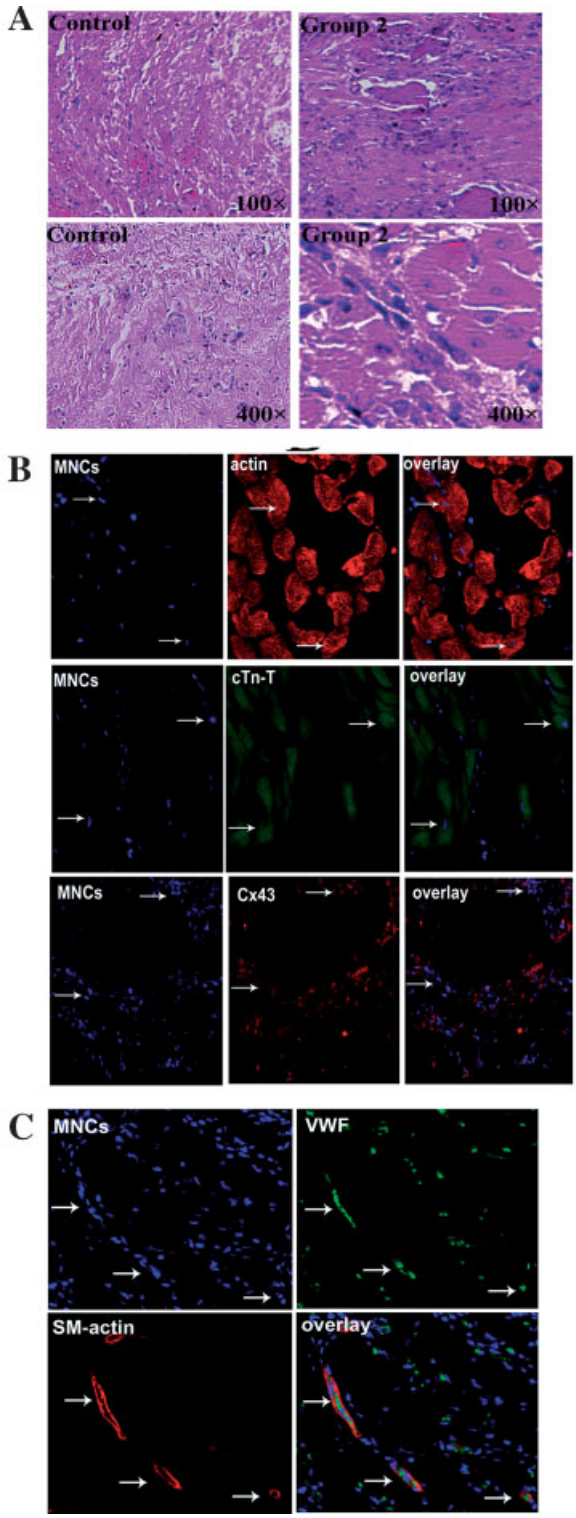

Fig. 4. Histological analysis after intracoronary delivery of MNCs. **A**: H&E staining showed that less fibrosis and more surviving myocardium could be observed in group 2 than that in group control. **B**: Transdifferentiation of implanted MNCs in group 2 in vivo. Several myocardium-specific proteins, including α-sarcomeric actin (actin), cardiac troponin T (cTn-T) and connexin 43 (Cx43), could be observed to express in DAPI-positive MNCs. **C**: Angiogenesis of implanted MNCs in vivo. Microvessel-specific proteins, including von Willebrand (VWF) and vascular smooth muscle actin (SM-actin), expressed in infarcted region in group 2. Final magnification for (B) and (C) was 400×.

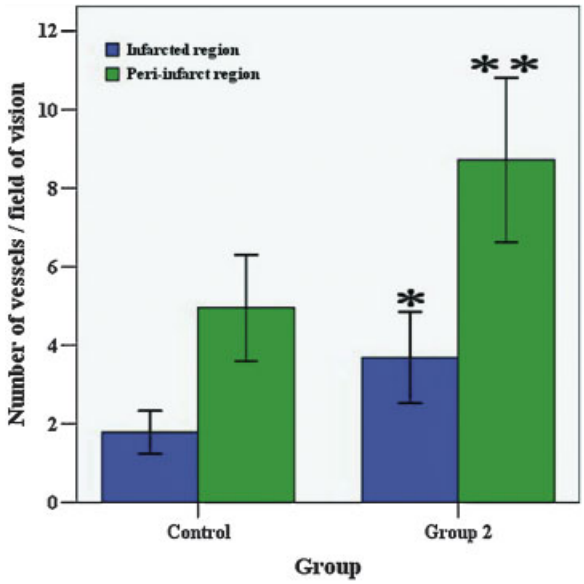

Fig. 5. Vascular densities in infarcted region and peri-infarct region in the endpoint. There were significant differences in vascular density of infarcted region between group control and group 2 in the endpoint ($^{*}P < 0.003$), also in peri-infarct region ($^{**}P < 0.003$). [Color figure can be viewed in the online issue, which is available at www.interscience.wiley.com.]

[Leri et al., 2002; Urbanek et al., 2003], (5) cell fusion of transplanted stem cells with resident myocytes [Oh et al., 2003], and (6) inhibition of cardiac apoptosis and fibrosis [Berry et al., 2006]. Our results indicate that MNCs take part in the former two mechanisms at least in some part.

The improvements in cardiac function of post-infarction hearts have been attributable to transdifferentiation by previous investigators [Orlic et al., 2001]; however, it has been questioned by recent experimental studies [Murry et al., 2004]. In addition, retention rate of infused cells in the hearts is so small that the significant improvements in cardiac function can not be fully attributed to transdifferentiations. Recently the paracrine mechanism of stem cells has been shown to play an important role in the repair of coronary microcirculation and local microenvironments and in stimulating residual normal myocytes for regeneration and proliferation and instrinsic myocardial stem cells for cell regeneration after AMI [Nadal-Ginard et al., 2003; Torella et al., 2004; Kajstura et al., 2005]. This regeneration of blood vessels and muscle cells is most pronounced in the peri-infarct region, which is consistent with our results of MRI and distribution.

The clinical significance of intracoronary infusion of autologous bone marrow-derived MNCs may be suitable for a large number of patients with AMI. It is conceivable that remodeling after infarction may be ameliorated by this procedure. Therefore, cell therapy may represent a new option of therapy in AMI.

However, it remains questions which type of stem cells and transplantation approach is the best; when is the best timing of transplantation after AMI; and how many cells is needed for individual patients, etc. All of these problems need to be resolved in the future.

Study Limitations

This animal study may not fully represent the patient's situation. However, the swine model of AMI and reperfusion closely mimics the clinical condition in patients with AMI and reperfusion. Because of the short physical half-life of 18F-FDG, we cannot investigate the delayed biodistribution of radiolabeled MNCs in vivo. In addition, the follow-up time is not long enough, thus incapable of dynamically investigating the benefits resulting from cellular cardiomyoplasty with MNCs.

ACKNOWLEDGMENTS

This work was supported by National Basic Research Program (973 Program) in China [2005CB523303, Ministry of Science and Technology]. We appreciated professor Yong-Jian Geng for carefully revising our manuscript.

REFERENCES

Allers C, Sierralta WD, Neubauer S, Rivera F, Minguell JJ, Conget PA. 2004. Dynamic of distribution of human bone marrow-derived mesenchymal stem cells after transplantation into adult unconditioned mice. Transplantation 78:503–508.

Becker W, Meller J. 2001. The role of nuclear medicine in infection and inflammation. Lancet Infect Dis 1:326–333.

Beltrami AP, Barlucchi L, Torella D, Baker M, Limana F, Chimenti S, Kasahara H, Rota M, Musso E, Urbanek K, Leri A, Kajstura J, Nadal-Ginard B, Anversa P. 2003. Adult cardiac stem cells are multipotent and support myocardial regeneration. Cell 114:763–776.

Berry MF, EnglerAJ,Woo YJ, PirolliTJ,Bish LT, Jayasankar V, Morine KJ, GardnerTJ,Discher DE, Sweeney HL. 2006. Mesenchymal stem cell injection after myocardial infarction improves myocardial compliance. Am J Physiol Heart Circ Physiol 290:H2196–H2203.

Britten MB, Abolmaali ND, Assmus B, Lehmann R, Honold J, Schmitt J, Vogl TJ, Martin H, Schachinger V,

Dimmeler S, Zeiher AM. 2003. Infarct remodeling after intracoronary progenitor cell treatment in patients with acute myocardial infarction (TOPCARE-AMI): Mechanistic insights from serial contrast-enhanced magnetic resonance imaging. Circulation 108:2212–2218.

Fernandez-Aviles F, San Roman JA, Garcia-Frade J, Fernandez ME, Penarrubia MJ, de la Fuente L, Gomez-Bueno M, Cantalapiedra A, Fernandez J, Gutierrez O, Sanchez PL, Hernandez C, Sanz R, García-Sancho J, Sanchez A. 2004. Experimental and clinical regenerative capability of human bone marrow cells after myocardial infarction. Circ Res 95:742–748.

Hofmann M, Wollert KC, Meyer GP, Menke A, Arseniev L, Hertenstein B, Ganser A, Knapp WH, Drexler H. 2005. Monitoring of Bone Marrow Cell Homing Into the Infarcted Human Myocardium. Circulation 111:2198–2202.

Hou D, Youssef EA, Brinton TJ, Zhang P, Rogers P, Price ET, Yeung AC, Johnstone BH, Yock PG, March KL. 2005. Radiolabeled cell distribution after intramyocardial, intracoronary, and interstitial retrograde coronary venous delivery implications for current clinical trials. Circulation 112 [Suppl I]:I-150–I-156.

Kajstura J, Rota M, Whang B, Cascapera S, Hosoda T, Bearzi C, Nurzynska D, Kasahara H, Zias E, Bonafe M, Nadal-Ginard B, Torella D, Nascimbene A, Quaini F, Urbanek K, Leri A, Anversa P. 2005. Bone marrow cells differentiate in cardiac cell lineages after infarction independently of cell fusion. Circ Res 96: 127–137.

Kamihata H, Matsubara H, Nishiue T, Fujiyama S, Tsutsumi Y, Ozono R, Masaki H, Mori Y, Iba O, Tateishi E, Kosaki A, Shintani S, Murohara T, Imaizumi T, Iwasaka T. 2001. Implantation of bone marrow mononuclear cells into ischemic myocardium enhances collateral perfusion and regional function via side supply of angioblasts, angiogenic ligands, and cytokines. Circulation 104:1046–1052.

Kang WJ, Kang HJ, Kim HS, Chung JK, Lee MC, Lee DS. 2006. Tissue distribution of 18F-FDG-labeled peripheral hematopoietic stem cells after intracoronary administration in patients with myocardial infarction. J Nucl Med 47:1295–1301.

Kocher AA, Schuster MD, Szabolcs MJ, Takuma S, Burkhoff D, Wang J, Homma S, Edwards NM, Itescu S. 2001. Neovascularization of ischemic myocardium by human bone marrow-derived angioblasts prevents cardiomyocyte apoptosis, reduces remodeling and improves cardiac function. Nat Med 7:430–436.

Leri A, Kajstura J, Anversa P. 2002. Myocyte proliferation and ventricular remodeling. J Card Fail 8: S518–S525.

Murry CE, Soonpaa MH, Reinecke H, Nakajima H, Nakajima HO, Rubart M, Pasumarthi KB, Virag JI, Bartelmez SH, Poppa V, Bradford G, Dowell JD, Williams DA, Field LJ. 2004. Haematopoietic stem cells do not transdifferentiate into cardiac myocytes in myocardial infarcts. Nature 428:664–668.

Nadal-Ginard B, Kajstura J, Leri A, Anversa P. 2003. Myocyte death, growth, and regeneration in cardiac hypertrophy and failure. Circ Res 92:139–150.

Oh H, Bradfute SB, Gallardo TD, Nakamura T, Gaussin V, Mishina Y, Pocius J, Michael LH, Behringer RR, Garry DJ, Entman ML, Schneider MD. 2003. Cardiac progenitor cells from adult myocardium: Homing, differentiation, and fusion after infarction. Proc Natl Acad Sci USA 100:12313–12318.

Orlic D, Kajustra J, Chimenti S, Limana F, Jakoniuk I, Quaini F, Nadal-Ginard B, Bodine DM, Leri A, Anversa P. 2001. Mobilized bone marrow cells repair the infarcted heart, improving function and survival. Proc Natl Acad Sci USA 98:10344–10349.

Penicka M, Widimsky P, Kobylka P, Kozak T, Lang O. 2005. Early tissue distribution of bone marrow mononuclear cells after transcoronary transplantation in a patient with acute myocardial infarction. Circulation 112:e63–e65.

Perin EC, Dohmann HF, Borojevic R, Silva SA, Sousa AL, Silva GV, Mesquita CT, Belem L, Vaughn WK, Rangel FO, Assad JA, Carvalho AC, Branco RV, Rossi MI, Dohmann HJ, Willerson JT. 2004. Improved exercise capacity and ischemia 6 and 12 months after transendocardial injection of autologous bone marrow mononuclear cells for ischemic cardiomyopathy. Circulation 110 [11 Suppl 1]:213–218.

Schuster MD, Kocher AA, Seki T, Martens TP, Xiang G, Homma S, Itescu S. 2004. Myocardial neovascularization by bone marrow angioblasts results in cardiomyocyte regeneration. Am J Physiol Heart Circ Physiol 287:H525–H532.

Strauer BE, Brehm M, Zeus T, Kostering M, Hernandez A, Sorg RV, Kogler G, Wernet P. 2002. Repair of infarcted myocardium by autologous intracoronary mononuclear bone marrow cell transplantation in humans. Circulation 106:1913–1918.

Suzuki K, Murtuza B, Fukushima S, Smolenski RT, Varela-Carver A, Coppen SR, Yacoub MH. 2004. Targeted cell delivery into infarcted rat hearts by retrograde intracoronary infusion: Distribution, dynamics, and influence on cardiac function. Circulation 110:II225–II230.

Tang YL, Zhao Q, Zhang YC, Cheng L, Liu M, Shi J, Yang YZ, Pan C, Ge J, Phillips MI. 2004. Autologous mesenchymal stem cell transplantation induces VEGF and neovascularization in ischemic myocardium. Regul Pept 117:3–10.

Torella D, Rota M, Nurzynska D, Musso E, Monsen A, Shiraishi I, Zias E, Walsh K, Rosenzweig A, Sussman MA, Urbanek K, Nadal-Ginard B, Kajstura J, Anversa P, Leri A. 2004. Cardiac stem cell and myocyte aging, heart failure, and insulin-like growth factor-1 overexpression. Circ Res 94:514–524.

Tse HF, Kwong YL, Chan JK, Lo G, Ho CL, Lau CP. 2003. Angiogenesis in ischaemic myocardium by intramyocardial autologous bone marrow mononuclear cell implantation. Lancet 361:47–49.

Urbanek K, Quaini F, Tasca G, Torella D, Castaldo C, Nadal-Ginard B, Leri A, Kajstura J, Quaini E, Anversa P. 2003. Intense myocyte formation from cardiac stem cells in human cardiac hypertrophy. Proc Natl Acad Sci USA 100:10440–10445.

Weidner N, Semple JP, Welch WR, Folkman J. 1991. Tumor angiogenesis and metastasis—Correlation in invasive breast carcinoma. N Engl J Med 324:1–8.

Wollert KC, Meyer GP, Lotz J, Ringes-Lichtenberg S, Lippolt P, Breidenbach C, Fichtner S, Korte T, Hornig B, Messinger D, Arseniev L, Hertenstein B, Ganser A, Drexler H. 2004. Intracoronary autologous bone-marrow cell transfer after myocardial infarction: The BOOST randomized controlled clinical trial. Lancet 364:141–148.